Mechatronics and Mechanical Engineering | Kielce University of Technology
Received: Dec 18 2025
Revised: Feb 13 2026
Accepted: May 31 2026
Published: Apr 01 2026

Mechanical Behavior of a Sierpiński Triangle – Inspired Construction

Mateusz Rudnik[1]

[1]Faculty of Mechatronics and Mechanical Engineering, Kielce University of Technology, Tysiąclecia Państwa Polskiego 7 Ave., 25-314 Kielce, Poland; mrudnik@tu.kielce.pl
* mrudnik@tu.kielce.pl

Abstract: This study investigated selected mechanical properties of Sierpiński-based structures subjected to static compression loading. Four geometric iterations (1IT – 4IT) were designed and manufactured using the MEX (Material Extrusion) process with a FlSun V400 3D printer and PLA+ material, and tested in three printing orientations (0°, 45°, and 90°). The experimental results were presented using column charts, enabling direct comparison of the effects of geometric iteration and printing orientation on the mechanical response of the specimens. The analysis demonstrated that geometric iteration was the dominant factor governing mechanical behavior. Fully solid specimens (1IT) exhibited the highest load – carrying capacity and energy absorption, reaching a maximum compressive force of approximately 35.1 kN and work values of up to about 868 J. The introduction of internal voids in porous configurations (2IT – 4IT) led to a substantial reduction in maximum force, displacement at peak load, and absorbed energy, regardless of printing orientation. The influence of printing orientation was pronounced for solid specimens but decreased with increasing porosity, indicating that geometry – driven reduction of the effective load – displacement cross – section dominated over manufacturing-induced anisotropy. Specimen mass and volume decreased systematically with successive iterations and remained largely independent of printing orientation. The results confirm the potential of Sierpiński – based fractal geometries for lightweight structural components under compressive loading.

Keywords: Sierpiński Triangle; Mechanical Properties; Fractal Structures; Numerical Analysis; Structural Lightness.

Nomenclature

PLA+	Polylactic acid +
STL	Standard Tessellation Language
MEX	Material Extrusion

1. Introduction

In recent years, additive manufacturing technology, especially the MEX (Material Extrusion) method, has been increasingly used for producing elements with complex geometry [1–3]. This method allows fast design and fabrication of specimens with different shapes, which are difficult to obtain using conventional manufacturing methods. One of the important issues related to 3D printing is the possibility of reducing the mass of elements while maintaining acceptable mechanical properties, which is important for lightweight engineering structures [4–6]. For this purpose, cellular structures are often used, which consist of repeating cells and are characterized by the presence of internal voids [7,8]. Such structures allow reduction of material consumption and overall mass, but at the same time they usually lead to a decrease in load – carrying capacity compared to solid structures [9,10]. The mechanical properties of cellular structures depend

Received: Dec 18 2025
Revised: Feb 13 2026
Accepted: May 31 2026
Published: Apr 01 2026

strongly on their geometry and porosity level; therefore, they are widely investigated in many studies [11–13]. One possible way of designing structures with variable porosity is the use of fractal geometries. In contrast to classical cellular structures, fractal structures do not always rely on a simple and regular repetition of a single cell, but rather on iterative modification of geometry. An example of such geometry is the Sierpiński triangle, which allows gradual introduction of holes into the structure and increasing porosity in subsequent iterations [14–16]. For this reason, fractal structures can be treated as an extension of classical cellular structures, although their mechanical behavior is still not fully understood. Static compression testing is one of the basic methods used to evaluate mechanical properties of materials and structures. It allows determination of parameters such as maximum force, displacement, and work performed during deformation of the specimen. In the case of parts manufactured using the MEX process, the printing orientation relative to the loading direction plays an important role, because the layered nature of the process leads to anisotropic mechanical behavior. As a result, the same geometry may show different mechanical response depending on the printing orientation.

Tree-like fractal geometries have recently been proposed as an alternative to conventional lattice structures in additively manufactured components, offering hierarchical load distribution and improved energy absorption capabilities. In contrast to regular cellular architectures, fractal-based internal structures enable gradual stress transfer through branching mechanisms, which may reduce stress concentrations and delay failure initiation. Such approaches demonstrate the growing interest in applying fractal principles to mechanical design, particularly in the context of optimizing strength-to-weight ratio and deformation behavior under complex loading conditions [17].

Fractal-based design methods enable the generation of porous structures with non-uniform and randomly distributed voids, which are difficult to achieve using conventional scaffold-based approaches. By applying mathematical procedures based on Iterative Function Systems (IFS), it is possible to control the level of self-similarity and thus regulate the porosity and spatial distribution of internal cavities. Such an approach expands the design possibilities in additive manufacturing and may lead to structures with tailored mass, stiffness, and load-transfer characteristics[18,19].

The aim of this study was to investigate the influence of geometric iteration of structures based on the Sierpiński triangle and the printing orientation on the mechanical properties of specimens subjected to static compression testing. Four geometric iterations, including a solid structure and structures with increasing porosity, were analyzed in three printing orientations relative to the build platform. The experimental results were presented in the form of column charts, which allows direct comparison of the influence of geometry and printing orientation on the obtained mechanical parameters as well as specimen mass and volume.

2. Research methodology

2.1. Samples preparation

The samples were designed based on the recursive formula (1), which defines the volume of a solid with a Sierpiński triangle as its base. This formulation describes the progressive material removal resulting from the fractal perforation process.

$$\forall_{n\in N_+} \exists \begin{cases} V_1 = HT(a_1) = \dfrac{Ha_1^2\sqrt{3}}{4} \\ V_n = V_{n-1} - 3H^{n-2}T(a_n),\ n \geq 2 \end{cases} \tag{1}$$

Mechatronics and Mechanical Engineering
Kielce University of Technology
Received: Dec 18 2025
Revised: Feb 13 2026
Accepted: May 31 2026
Published: Apr 01 2026

where: V_1 – volume of the full (non-perforated) model; H – model height; a_1 – width of the initial triangular base; V_n – volume after the n-th iteration; V_{n-1} – volume of the previous iteration; n – iteration numer; a_n – width of each triangular void generated during perforation; $T(a_n)$ – area of the triangular perforation.

The initial side length was a_1 = 40 mm, while the subsequent iterations had side lengths

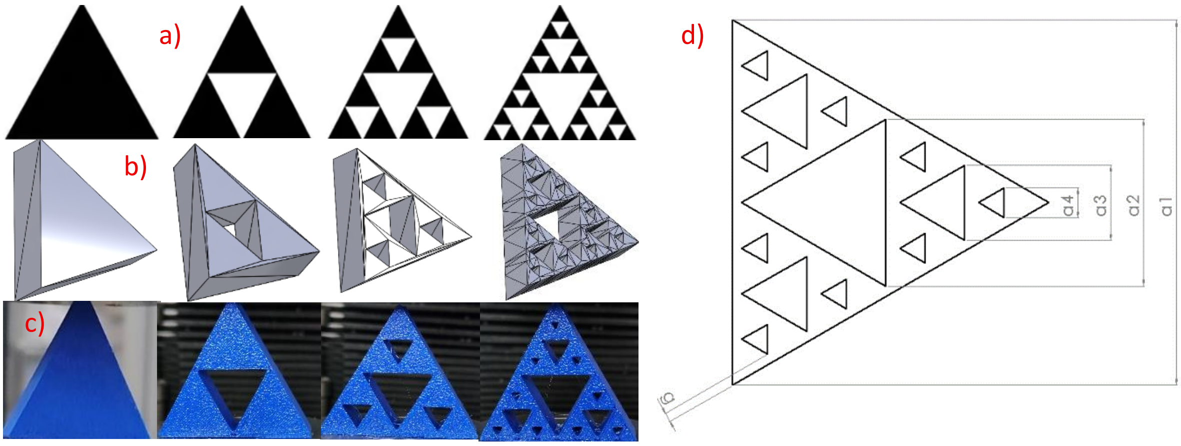

Figure 1. *Iterative geometry of the Sierpiński triangle–based structure: (a) 2D representations, (b) STL models, (c) manufactured samples, (d) dimensional scheme.*

of a_2 = 18.27 mm, a_3 = 8.27 mm, and a_4 = 3.3 mm, with a constant height of H = 10 mm and g = 1 mm. The models were manufactured using an FlSun V400 3D printer. The compression test for the first – iteration sample was performed on a UTS – 100 testing machine, whereas the following iterations were examined using an Inspekt Mini 3 kN testing system (Figure 1). The volume of the first – iteration sample is approximately $V_1 \approx 6928$ mm^3 (100%, no material loss). In the second iteration, the volume decreases to $V_2 \approx 5483$ mm^3 (79.14%, loss of 20.86%); in the third iteration to $V_3 \approx 4594$ mm^3 (66.31%, loss of 33.69%); and in the fourth iteration to $V_4 \approx 4170$ mm^3 (60.19%, loss of 39.81%).

2.2. Material and Experimental Equipment

PLA material

PLA+ by eSUN is a modified polylactide intended for MEX printing, with a density of approximately 1.23 g/cm^3. The tensile strength is typically 60 – 63 MPa, while the elongation at break is about 15 – 20%, indicating reduced brittleness compared to standard PLA. The flexural strength is approximately 70 – 75 MPa, and the flexural modulus ranges from 2.0 to 2.9 GPa. The heat deflection temperature (HDT, 0.45 MPa) is approximately 53 °C. The material exhibits a melt flow index of MFI ≈ 5 g/10 min (190 °C / 2.16 kg). The recommended

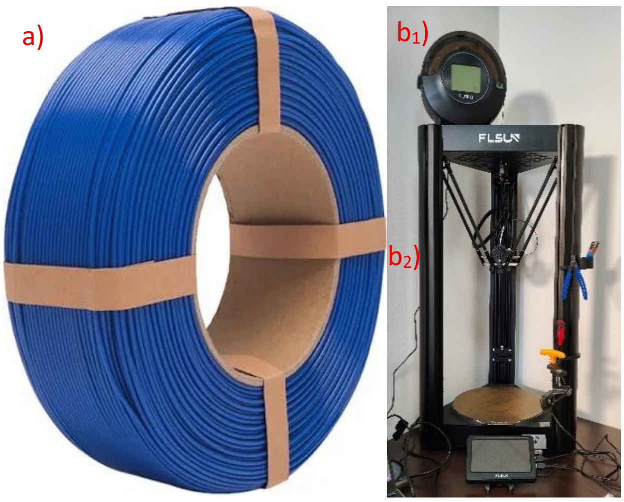

Figure 2. *a) PLA+ – Blue material; b_1) SUNLU FilaDryer S2 b_2) FlSun v400*

Mechatronics and Mechanical Engineering
Kielce University of Technology
Received: Dec 18 2025
Revised: Feb 13 2026
Accepted: May 31 2026
Published: Apr 01 2026

extrusion temperature is 210 – 230 °C, and the build plate temperature is 45 – 60 °C [20].

3D Printer – FlSun v400

The FlSun V400 is a 3D printer operating in MEX technology, based on a delta – type kinematic structure. The build volume has a cylindrical shape with a diameter of approximately 300 mm and a height of about 410 mm. The device is designed to process 1.75 mm filament and supports common thermoplastic materials, including PLA, PLA+, PETG, ABS, and TPU. The maximum hotend temperature is approximately 300 °C, while the heated bed reaches temperatures of up to about 110 °C. The printer is equipped with a direct – drive extruder and an automatic bed – leveling system. Control is implemented via Klipper firmware, enabling operation at high printing speeds, declared to reach up to approximately 400 mm/s, while maintaining control over motion and extrusion parameters (Figure b_2) [21–23].

SUNLU FilaDryer S2 – filament dryer

The SUNLU FilaDryer S2 is a device designed for drying and conditioning filaments used in FDM/FFF technology. The dryer features a closed chamber accommodating one standard filament spool (1.75 mm or 2.85 mm) with a maximum diameter of approximately 210 mm. The operating temperature range is approximately 35 – 70 °C, allowing moisture removal from typical polymer materials such as PLA, PLA+, PETG, ABS, TPU, and nylon. Heating is applied uniformly within the chamber, and operating parameters (temperature and drying time) are set via a control panel with a display. The device can be used both prior to printing and during printing, providing stable conditions for the filament (Figure b_1) [24].

UTS – 100 – Testing Machine

The UTS – 100 is an electromechanical universal testing machine intended for static mechanical testing of materials. The device is characterized by a maximum load capacity of approximately 100 kN and enables tensile, compression, and bending tests, depending on the applied fixtures. The machine is equipped with a load cell and a crosshead displacement measurement system, allowing the acquisition of force – displacement characteristics. The loading rate is controlled electromechanically and set via the control system, while test results are recorded digitally for further analysis (Figure 3a) [25].

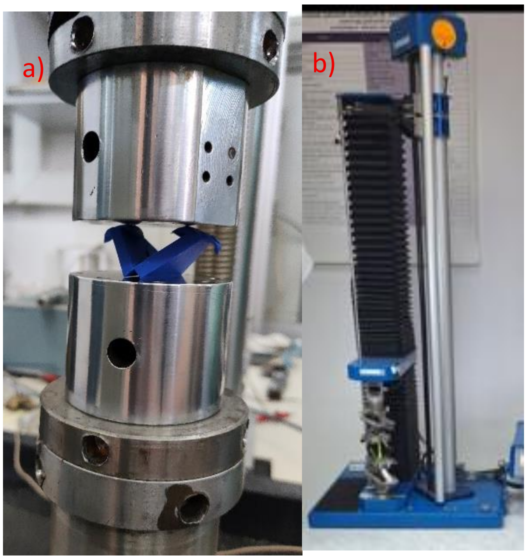

Figure 3. *a) UTS – 100; b) Inspekt Mini 3kN.*

Inspekt Mini 3 kN – Testing Machine

The Inspekt Mini 3 kN is an electromechanical testing machine with a maximum load capacity of 3 kN, designed for mechanical testing of small – scale specimens. The device enables tensile and compression tests with simultaneous measurement of force and displacement. The construction includes a load – displacement frame with a drive system, a load cell with a 3 kN range, and a deformation measurement system (Figure 3b). Control is performed via computer software (Labmaster), allowing adjustment of the loading rate and digital acquisition of test data [26].

M&ME
Mechatronics and Mechanical Engineering
Kielce University of Technology
Received: Dec 18 2025
Revised: Feb 13 2026
Accepted: May 31 2026
Published: Apr 01 2026

2.3. STL Model Definition, Additive Manufacturing Parameters, and Compression Test Conditions.

Although a formal statistical Design of Experiments (DoE) framework was not implemented, the experimental plan followed a structured parametric matrix in which two independent variables were systematically varied: print orientation (0°, 45°, 90°) and fractal iteration level (1IT, 2IT, 3IT, 4IT). This produced 12 distinct experimental configurations. Such a matrix-based approach ensured controlled and repeatable variation of geometric and process parameters, enabling a consistent comparative mechanical evaluation of the samples (Table 1).

Table 1. Experimental matrix showing the combinations of printing orientation and fractal iteration level

Printing orientation	0°	45°	90°	0°	45°	90°	0°	45°	90°	0°	45°	90°
Type of sample	1IT	2IT	3IT	4IT	1IT	2IT	3IT	4IT	1IT	2IT	3IT	4IT

The specimens were designed as STL files with increasing geometric complexity corresponding to four iterations (1IT – 4IT). The 1IT geometry consisted of 8 triangular facets, while the 2IT, 3IT, and 4IT models contained 24, 72, and 520 triangular facets, respectively. For all STL files, the same geometric tolerance of 0.025 was applied to ensure consistent surface accuracy across iterations.

All specimens were manufactured using the Orca Slicer software with identical printing parameters. The printing configuration included four top layers and four bottom layers, as well as three wall loops. The layer height was set to 0.2 mm, with the first layer height also equal to 0.2 mm. A linear infill pattern with a nominal infill density of 100% was used. Support structures were generated only when required by the geometry. The travel speed was set to 400 mm/s. The printing speed for the external walls was 120 mm/s, while the internal walls were printed at 200 mm/s. The infill printing speed was set to 250 mm/s. The first layer was printed at a reduced speed of 50 mm/s, with the first – layer infill speed set to 100 mm/s to ensure adequate adhesion to the build platform. Specimens were manufactured in three printing orientations relative to the build platform, namely 0°, 45°, and 90°, as illustrated in Figure 4.

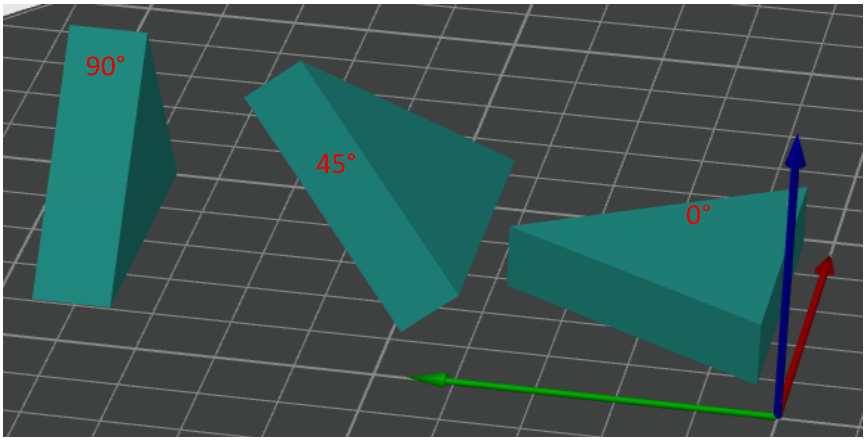

Figure 4*. Arrangement of the specimens on the build platform.*

Static compression tests were conducted in accordance with ISO 604. The tests were performed at a constant crosshead speed of 5 mm/min. Each test was terminated when an 80% drop in force relative to the maximum recorded value was observed, which was taken as the failure criterion [27].

Mechatronics
and Mechanical Engineering

Kielce
University of Technology

Received: Dec 18 2025
Revised: Feb 13 2026
Accepted: May 31 2026
Published: Apr 01 2026

3. Results and Discussion

Figure 5a shows curves for 1IT specimens printed at orientations of 0°, 45°, and 90°. An increase in load-displacement capacity is observed with changing orientation, with the specimen printed at

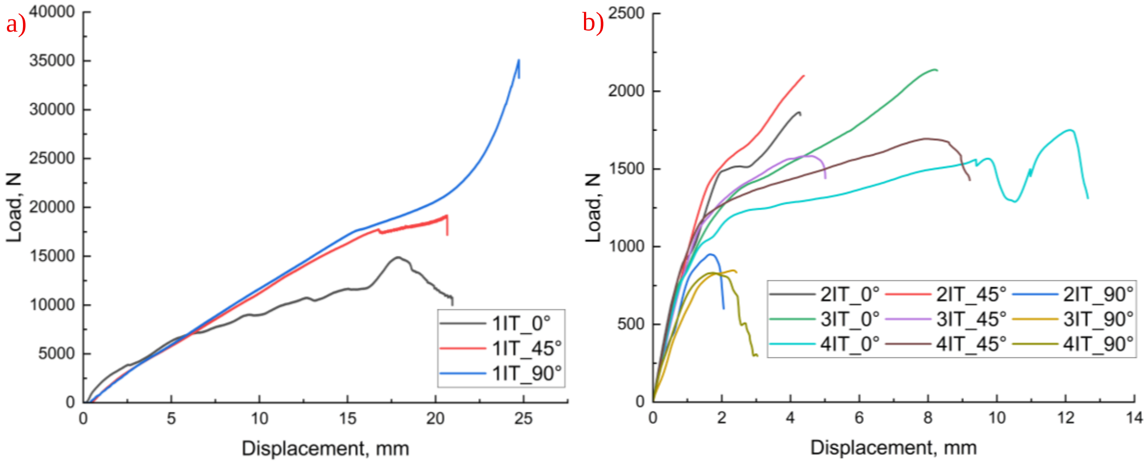

Figure 5. *Load–displacement curves for specimens with different structural configurations and printing orientations: a) Solid samples (1IT); b) Samples with holes (2IT, 3IT, 4IT).*

90° reaching the highest load values and the greatest displacement prior to failure. Figure 5b presents curves for 2IT, 3IT, and 4IT specimens printed at orientations of 0°, 45°, and 90°. The responses are nonlinear and exhibit local load drops, indicating progressive structural degradation. Differences in maximum load and stiffness reflect the influence of both geometric configuration and layer orientation on the deformation mechanism. Such nonlinear behavior and progressive degradation are consistent with observations reported for fractal porous structures, where internal hierarchical geometry governs load redistribution.

Figures 6a – f presented the results of the static compression tests performed on single specimens manufactured in four geometric iterations (1IT – 4IT) and in three printing orientations (0°, 45°, and 90°). It was emphasized that the reported values were not averaged results but corresponded to a single specimen for each combination of iteration and printing orientation. This approach enabled a direct assessment of the influence of internal geometry and additive manufacturing – induced anisotropy on the mechanical response of the structures. A similar geometry-focused assessment is commonly applied in studies of fractal-based porous structures to isolate the mechanical contribution of hierarchical internal architecture.

Figure 6a compared the maximum compressive force obtained during testing. The 1IT specimens, representing fully solid samples, exhibited by far the highest load – displacement capacity in all printing orientations. A pronounced increase in the maximum force was observed with the change in orientation from 0° (F_{max} ≈ 10.8 kN) to 45° (F_{max} ≈ 19.2 kN) and further to 90° (F_{max} ≈ 35.1 kN). In subsequent iterations (2IT – 4IT), where internal holes were introduced and porosity was increased, a sharp reduction in the maximum force occurred, dropping below approximately 2.2 kN for 2IT, to about 0.9 – 2.1 kN for 3IT, and below 1.8 kN for 4IT. The effect of geometric iteration was clearly more pronounced than the effect of printing orientation in perforated samples, indicating that the reduction of the effective load – displacement cross – section dominated over anisotropy related to layer orientation. This dominance of geometric perforation over orientation effects aligns with behavior observed in fractal porous architectures, where strength is primarily controlled by hierarchical void distribution.

Mechatronics and Mechanical Engineering | Kielce University of Technology | Received: Dec 18 2025
Revised: Feb 13 2026
Accepted: May 31 2026
Published: Apr 01 2026

Figure 6b showed the displacement corresponding to the maximum compressive force. The 1IT specimens exhibited the largest displacements, which increased with orientation from approximately 12.7 mm at 0° to 20.7 mm at 45° and 24.7 mm at 90°, indicating a higher deformation capacity prior to loss of load – displacement ability. In the 2IT – 4IT specimens, the displacements were significantly reduced, generally remaining below 9 mm and decreasing below 2.5 mm in the 90° orientation. The 0° orientation allowed larger deformation compared to 90°, which suggested increased directional stiffness when the layer arrangement was unfavorable with respect to the loading direction. Comparable orientation-dependent deformation responses have been reported in additively manufactured fractal porous structures, where anisotropy interacts with hierarchical geometry.

Figure 6c presented the mass of individual specimens. The 1IT samples showed the highest mass, approximately 8.4 – 8.5 g, with only minor variations between printing orientations. Introducing internal voids in iterations 2IT – 4IT resulted in a systematic reduction in mass, to approximately 6.6 – 6.7 g for 2IT and about 5.6 g for 3IT. The influence of printing orientation on mass was negligible and mainly resulted from manufacturing tolerances. Such controlled mass reduction reflects geometry-driven porosity evolution typical of fractal structural modeling approaches.

Received: Dec 18 2025
Revised: Feb 13 2026
Accepted: May 31 2026
Published: Apr 01 2026

Figure 6d illustrated the geometric volume of the specimens for successive iterations. A clear monotonic decrease in volume was observed, from 6.93 cm³ for 1IT samples to 5.48 cm³ for 2IT and approximately 4.60 cm³ for 3IT and 4IT. This parameter was independent of printing orientation, as the specimen geometry remained unchanged and only the build orientation within the printing chamber varied. This behavior mirrors fractal-based design principles in which internal

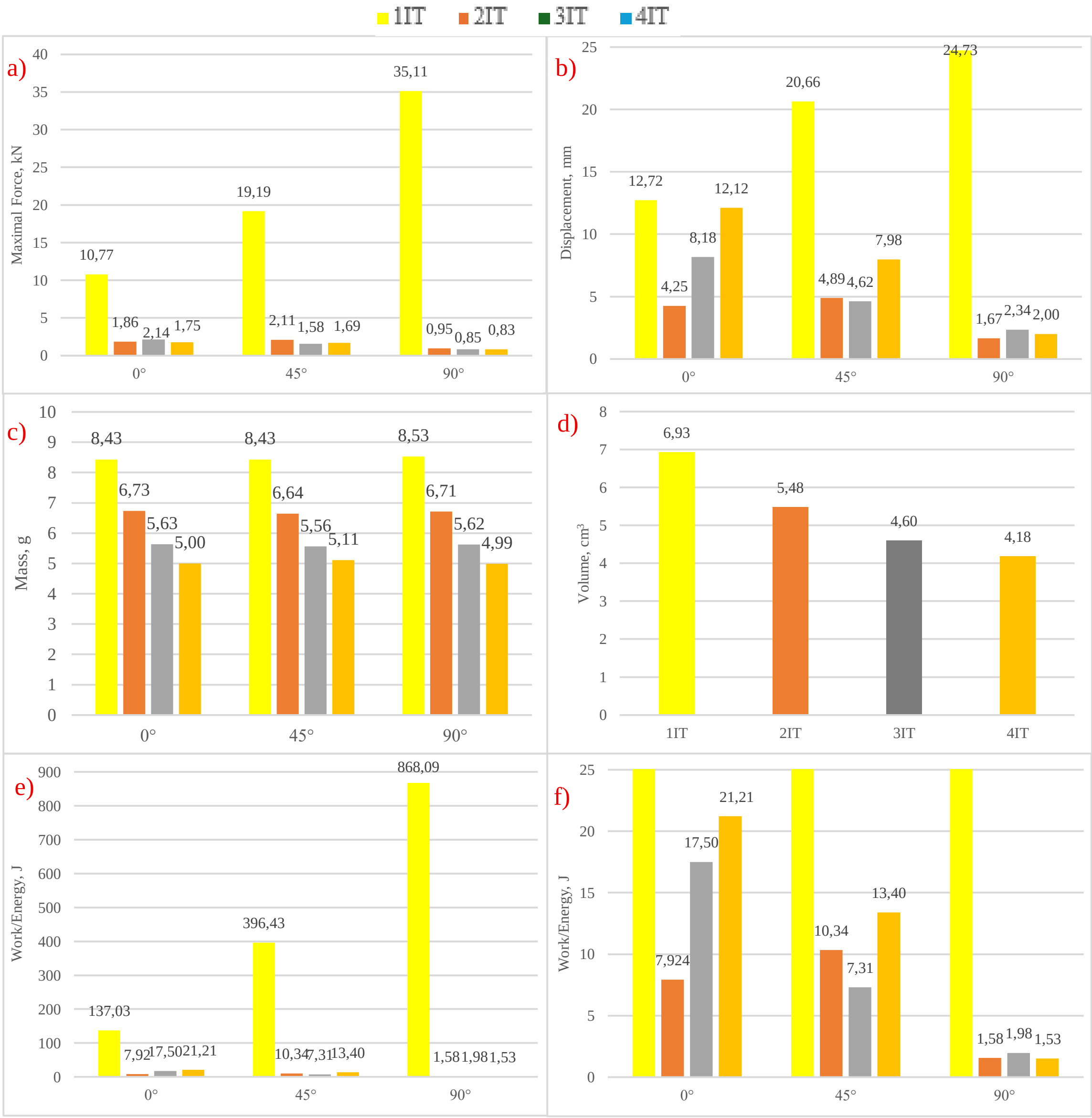

Figure 6. *Column charts showing the results of the static compression tests: a) maximum compressive force; b) displacement at the maximum force; c) specimen mass; d) specimen volume; e) work (energy) absorbed during compression; f) enlarged view of Figure 4e highlighting the lower work values obtained for the subsequent geometric iterations.*

void generation modifies material distribution without altering global geometry.

Figures 6e and 6f presented the work performed during compression. Figure 6e covered the full range of results and demonstrated that the 1IT specimens possessed a markedly higher energy absorption capacity than the perforated structures, particularly in the 90° orientation, where the work reached approximately 868 J, compared with about 137 J at 0° and 396 J at 45°. Figure 6f provided a magnified view of the lower work range, which enabled a detailed analysis of iterations

Received: Dec 18 2025
Revised: Feb 13 2026
Accepted: May 31 2026
Published: Apr 01 2026

2IT – 4IT. In this group, the work values decreased to the order of several to a few tens of joules, and a further reduction was observed with increasing porosity and unfavorable printing orientation, indicating earlier loss of load – displacement capacity and limited energy accumulation in geometrically complex structures. This reduction in energy absorption is consistent with findings for hierarchical fractal porous systems, where internal geometry governs energy dissipation mechanisms [19].

A comparable tendency toward progressive and uniform deformation of hierarchical fractal structures under mechanical loading has been reported for tree-like fractal architectures manufactured via Selective Laser Melting, where branching geometry enabled predictable stress redistribution during flexural testing. Similarly to the SLM-based tree-like fractal study, the present results indicate that hierarchical internal geometry plays a dominant role in governing mechanical response and energy absorption, while geometric parameters control the stress–strain evolution more strongly than manufacturing-induced anisotropy in highly perforated configurations [17].

4. Conclusions

Based on the results of the static compression tests performed on single specimens manufactured in four geometric iterations (1IT – 4IT) and in three printing orientations (0°, 45°, and 90°), the following conclusions were drawn:

- Geometric iteration was the primary factor determining the mechanical response of the specimens, with solid structures (1IT) exhibiting the highest load – displacement capacity
  and the greatest energy absorption capability compared to porous configurations (2IT – 4IT).
- The addition of holes and increased porosity lead to a significant decrease in maximum force, displacement at ultimate load, and work done during compression, regardless of the orientation of the print.
- Printing orientation affected the maximum force and work values; however, its influence decreased with increasing structural porosity, and in perforated specimens the effect of geometry dominated over the anisotropy induced by the additive manufacturing process.
- Solid specimens exhibited a greater deformation capacity prior to loss of load – displacement ability, as confirmed by higher displacement values compared to specimens with porous structures.
- The mass and volume of the specimens decreased systematically in subsequent iterations in accordance with the design assumptions, while these parameters remained practically independent of the printing orientation.

Author Contributions: Conceptualization, M.R.; methodology, M.R.; software, M.R.; validation, M.R.; formal analysis, M.R.; investigation, M.R.; resources, M.R.; data curation, M.R.; writing—original draft preparation, M.R.; writing—review and editing, M.R.; visualization, M.R.; supervision, M.R.; project administration, M.R.; funding acquisition, M.R.

Funding: This research received no external funding.

Conflicts of Interest: The authors declare no conflict of interest.

Received: Dec 18 2025
Revised: Feb 13 2026
Accepted: May 31 2026
Published: Apr 01 2026

Acknowledgments:
The author would like to thank the Laboratory of Experimental Mechanics for performing the mechanical tests and providing technical support during the experimental investigations.

References

1. Marabello, G.; Chairi, M.; Parisi, M.; Di Bella, G. Influence of Layer Thickness and Extrusion Temperature on the Mechanical Behavior of PLA–Flax TPMS Sandwich Structures Fabricated via Fused Filament Fabrication. *Materials* **2025**, *18*, 5356, doi:10.3390/ma18235356.
2. Bandinelli, F.; Ciampaglia, A.; Ciardiello, R.; Peroni, L.; Peroni, M.; Scapin, M. High Strain Rate Testing of Carbon-Epoxy Laminate Crash Boxes Filled with Polymeric Cellular 3D-Printed Cores. *Int. J. Impact Eng.* **2025**, *205*, 105401, doi:10.1016/j.ijimpeng.2025.105401.
3. Koroľ, M.; Török, J.; Monka, P.P.; Baron, P.; Mrugalska, B.; Monkova, K. Researching on the Effect of Input Parameters on the Quality and Manufacturability of 3D-Printed Cellular Samples from Nylon 12 CF in Synergy with Testing Their Behavior in Bending. *Polymers (Basel).* **2024**, *16*, 1429, doi:10.3390/polym16101429.
4. Mencarelli, M.; Sisella, M.; Puggelli, L.; Innocenti, B.; Volpe, Y. Sensitivity Analysis of 3D Printing Parameters on Mechanical Properties of Fused Deposition Modeling-Printed Polylactic Acid Parts. *Applied Mechanics* **2025**, *6*, 17, doi:10.3390/applmech6010017.
5. Kumar, A.P.; Kumar, M.D.B.; Sreekanth, P.S.R.; Sahu, S.K.; Ma, Q.; Hanon, M.M.; Aman, M. Experimental Investigation on the Transverse Crushing Performance of 3D Printed Polymer Composite Filled Aluminium Tubes. *J. Mech. Behav. Mater.* **2025**, *34*, doi:10.1515/jmbm-2025-0091.
6. Małek, M.; Kluczyński, J.; Jasik, K.; Kardaszuk, E.; Szachogłuchowicz, I.; Łuszczek, J.; Torzewski, J.; Grzelak, K.; Ewiak, I. An Eco-Friendly and Innovative Approach in Building Engineering: The Production of Cement–Glass Composite Bricks with Recycled Polymeric Reinforcements. *Materials* **2024**, *17*, 704, doi:10.3390/ma17030704.
7. Akçay, Ö.; Arı, A. Effect of Infill Density and Infill Pattern on Mechanical Properties of 3D-Printed PLA Produced by FFF. *Fırat Üniversitesi Mühendislik Bilimleri Dergisi* **2025**, *37*, 223–232, doi:10.35234/fumbd.1538296.
8. Czech, K.; Krajewski, D.; Oleksy, M. Sandwich Composites Containing Thermoplastic Core Structures Manufactured by 3D Printing for Defense Industry Applications. *Chemical and Process Engineering: New Frontiers* **2025**, 92–92, doi:10.24425/cpe.2025.153677.
9. Hulea, R.; Stefan, R.; Kiss, I.-A.; Ariesan, R.A. Combined Influence of 3D Printing Parameters and Thermal Conditioning on the Tensile Strength of FGF-Printed PLA Components. *Journal of Polymer Research* **2025**, *32*, 387, doi:10.1007/s10965-025-04620-9.
10. Taşdemir, M.; Toktaş, İ.; Motameni, A.; Evis, Z. Experimental and Numerical Investigation of Mechanical Properties of PLA-Based Auxetic Structures. *The International Journal of Advanced Manufacturing Technology* **2025**, *137*, 83–103, doi:10.1007/s00170-025-15141-6.
11. Gontarz-Kulisiewicz, M.E.; Budzik, G.; Dziubek, T.; Sobolewski, B.; Przeszłowski, Ł. The Influence of Polymer Materials and Internal Density on the Parameters of Fused Filament Fabrication Samples during Tensile Testing. *Advances in Science and Technology Research Journal* **2025**, *19*, 410–427, doi:10.12913/22998624/207875.

Received: Dec 18 2025
Revised: Feb 13 2026
Accepted: May 31 2026
Published: Apr 01 2026

12. Liu, T.; Chen, K. Influence of LLDPE on the Mechanical Properties Improvement of 3D Printed POE/LLDPE Blends. *Journal of Vinyl and Additive Technology* **2024**, *30*, 983–996, doi:10.1002/vnl.22099.

13. Cañero-Nieto, J.M.; Campo-Campo, R.J.; Díaz-Bolaño, I.; Ariza-Echeverri, E.A.; Deluque-Toro, C.E.; Solano-Martos, J.F. Infill Pattern Strategy Impact on the Cross-Sectional Area at Gauge Length of Material Extrusion 3D Printed Polylactic Acid Parts. *J. Intell. Manuf.* **2025**, doi:10.1007/s10845-025-02579-4.

14. Rojo-Francàs, A.; Pansari, P.; Bhattacharya, U.; Juliá-Díaz, B.; Grass, T. Anomalous Quantum Transport in Fractal Lattices. *Commun. Phys.* **2024**, *7*, 259, doi:10.1038/s42005-024-01747-x.

15. Kigami, J.; Takahashi, K. "The Sierpinski Gasket Minus Its Bottom Line" as a Tree of Sierpinski Gaskets. *Mathematische Zeitschrift* **2024**, *306*, 28, doi:10.1007/s00209-023-03416-1.

16. Patiño Ortiz, J.; Patiño Ortiz, M.; Martínez-Cruz, M.-Á.; Balankin, A.S. A Brief Survey of Paradigmatic Fractals from a Topological Perspective. *Fractal and Fractional* **2023**, *7*, 597, doi:10.3390/fractalfract7080597.

17. Stanciu Birlescu, A.; Vilau, C.; Balc, N. Analysis of the Mechanical Behavior of Tree-like Fractal Structures in SLM-Manufactured Components. *Materials* **2025**, *18*, 2215, doi:10.3390/ma18102215.

18. Mollinedo, H.; Pineda León, E.; De-León, D.; Kryvko, A.; Miguel-Andrés, I.; Samayoa, D.; Damián-Adame, L. The Fractal Timoshenko Beam Equation. *Fractal and Fractional* **2026**, *10*, 65, doi:10.3390/fractalfract10010065.

19. Ullah, A.S.; D'Addona, D.M.; Seto, Y.; Yonehara, S.; Kubo, A. Utilizing Fractals for Modeling and 3D Printing of Porous Structures. *Fractal and Fractional* **2021**, *5*, 40, doi:10.3390/fractalfract5020040.

20. PLA+ ESUN, Technical Data Sheet, Https://3d.Nice-Cdn.Com/Upload/File/ESUN_PLA_-Filament_TDS_V4.0[2].Pdf, 18.12.2025.

21. FlSun V400, Https://Github.Com/Phnxdrgn536/FLSun-V400/Blob/Main/FlsunV400-English-Instruction-Manual.Pdf, 18.12.2025.

22. Ratiu, M.; Prichici, M.A.; Anton, D.M.; Negrau, D.C. Tensile Testing of Samples Printed on Delta and Cartesian 3D Printer. *IOP Conf. Ser. Mater. Sci. Eng.* **2022**, *1256*, 012018, doi:10.1088/1757-899X/1256/1/012018.

23. Zhuk, Y.; Klotchko, T. COMPARISON OF 3D-PRINTED PARTS' QUALITY USING PRINTERS WITH "COREXY" AND "DELTA" KINEMATICS. *Bulletin of Kyiv Polytechnic Institute. Series Instrument Making* **2024**, 50–55, doi:10.20535/1970.68(2).2024.318630.

24. SUNLU FilaDryer S2, Https://Www.Instrukcjaobslugipdf.Pl/Sunlu/Filadryer-S2/Instrukcja, 18.12.2025.

25. KATALOG WYPOSAŻENIA LABORATORIÓW NAUKOWO-BADAWCZYCH I DYDAKTYCZNYCH CZĘŚĆ II, UTS - 100, Https://Wmibm.Tu.Kielce.Pl/Wp-Content/Uploads/2016/11/Katalog_lab_cz2.Pdf.

Mechatronics
and Mechanical Engineering

Kielce
University of Technology

Received: Dec 18 2025
Revised: Feb 13 2026
Accepted: May 31 2026
Published: Apr 01 2026

26. Inspekt Mini 3kN, Https://Www.Hegewald Peschke.Com/Products/Universal-Testing-Machines/Testing-Applications/Product-Detail/Testing Equipment-for-the-Determination-of-Adhesion-Forces/, .

27. ISO 604 Plastics — Determination of Compressive Properties.